Atmospheric Research 240 (2020) 104948

Contents lists available at ScienceDirect

Atmospheric Research

journal homepage: www.elsevier.com/locate/atmosres

Changes in inorganic aerosol compositions over the Yellow Sea area from impact of Chinese emissions mitigation

Yu-Jin Jo[a], Hyo-Jung Lee[b,**], Hyun-Young Jo[b], Jung-Hun Woo[c], Younha Kim[d], Taehyoung Lee[e], Gookyoung Heo[f], Seung-Myung Park[g], Donghee Jung[g], Jihoon Park[g], Cheol-Hee Kim[a,*]

[a] Department of Atmospheric Sciences, Pusan National University, Busan, Republic of Korea
[b] Institute of Environmental Studies, Pusan National University, Busan, Republic of Korea
[c] Department of Advanced Technology Fusion, Konkuk University, Seoul, Republic of Korea
[d] International Institute for Applied Systems Analysis (IIASA), Laxenburg, Austria
[e] Department of Environmental Science, Hankuk University of Foreign Studies, Yongin, Republic of Korea
[f] National Center for Fine Dust Information, Ministry of Environment, Cheongju, Republic of Korea
[g] Climate and Air Quality Research Department, National Institute of Environmental Research, Incheon, Republic of Korea

ARTICLE INFO

Keywords:
Inorganic aerosol
Chinese emissions mitigation
Yellow Sea
Baengnyeong supersite

ABSTRACT

Substantial mitigation of air pollutants emissions has been performed since 2013 around Beijing, and changes in the atmospheric characteristics have been expected over the downstream area of Beijing. In this study, both WRF-Chem simulation and on-site measurements were utilized for the Baengnyeong (island) supersite, one of the representative regional background sites located in the Yellow Sea, the entrance area of the long-range transport process in Korea. The changes in the chemical compositions of inorganic aerosols were examined for spring-time during the Chinese emission mitigation period from 2014 to 2016.

The measured ratio of ionic species to $PM_{2.5}$ at the Baengnyeong supersite showed changes in aerosol inorganic chemical compositions from sulfate in 2014 to nitrate in 2015–2016. The modeling results also showed that nitrate was low in 2014 and significantly increased in 2015 and 2016, and the acidic aerosol condition had also changed toward a more neutralized status in both the simulation and the observations. The WRF-Chem modeling study further indicated that the sulfur was not neutralized in 2014. However, in 2015 and 2016, SO_2 was more sufficiently neutralized as sulfur emissions were substantially reduced in China, while at the same time nitrate had begun to increase in such a 'SO_2–poor' condition in Beijing area in China, and thus approaching more enhanced neutralization over the Yellow Sea area. The causes of the higher nitrate based on the modeled characteristics of the ammonia-sulfate-nitrate aerosol formation in response to the SO_2 emissions reduction in China are also discussed in this paper.

1. Introduction

Particulate matter (PM) is recognized to have a substantial impact on the environment and is of concern for health-related effects (Marcazzan et al., 2001), and climate and air quality (Fuzzi et al., 2015). PM also has become a significant issue associated with transboundary pollution over Northeast Asia (Chiashi et al., 2019; Shapiro, 2016). In early 2013, high-emission areas such as Beijing, Hebei, and other regions in China suffered from persistent haze (MEE, 2019), and the Chinese government issued China's first 5-year Clean Air Action Plan for the period 2013 to 2017 as part of the Prevention and Control of Air Pollution (PCAP) (China State Council, 2013; http://www.sustainabletransport.org/archives/1563; Jin et al., 2016), a crucial strategic plan in China for comprehensive emissions control. As a result, it was reported that the Chinese air quality had been significantly improved with a decrease in the average concentration of PM_{10} nationwide. Numerous space- and ground-based observations have reported the improvement in China's air quality in response to the PCAP (Krotkov et al., 2016; Liu et al., 2016; Zhang et al., 2017; Zhao et al., 2017; Zheng et al., 2018a).

* Correspondence to: C.-H. Kim, Department of Atmospheric Sciences, Pusan National University, 30 San, Jangjeon-Dong, Geumjeong-Gu, Busan 609-735, Republic of Korea.
** Correspondence to: H.-J. Lee, Institute of Environmental Studies, Pusan National University, 30 San, Jangjeon-Dong, Geumjeong-Gu, Busan 609-735, Republic of Korea.
E-mail addresses: hyojung@pusan.ac.kr (H.-J. Lee), chkim2@pusan.ac.kr (C.-H. Kim).

https://doi.org/10.1016/j.atmosres.2020.104948
Received 27 November 2019; Received in revised form 15 February 2020; Accepted 9 March 2020
Available online 10 March 2020

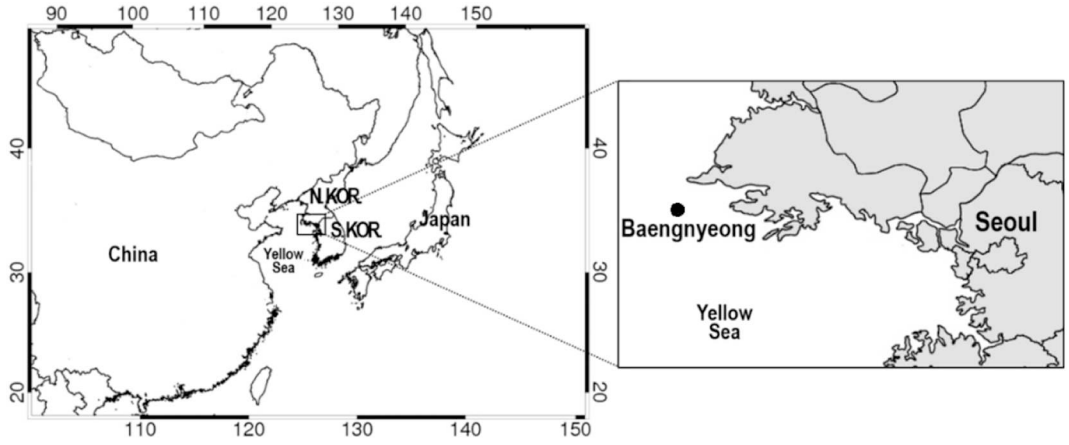

Fig. 1. WRF-Chem model domain and location of the Baengnyeong supersite (refered to as 'B-site' in the text).

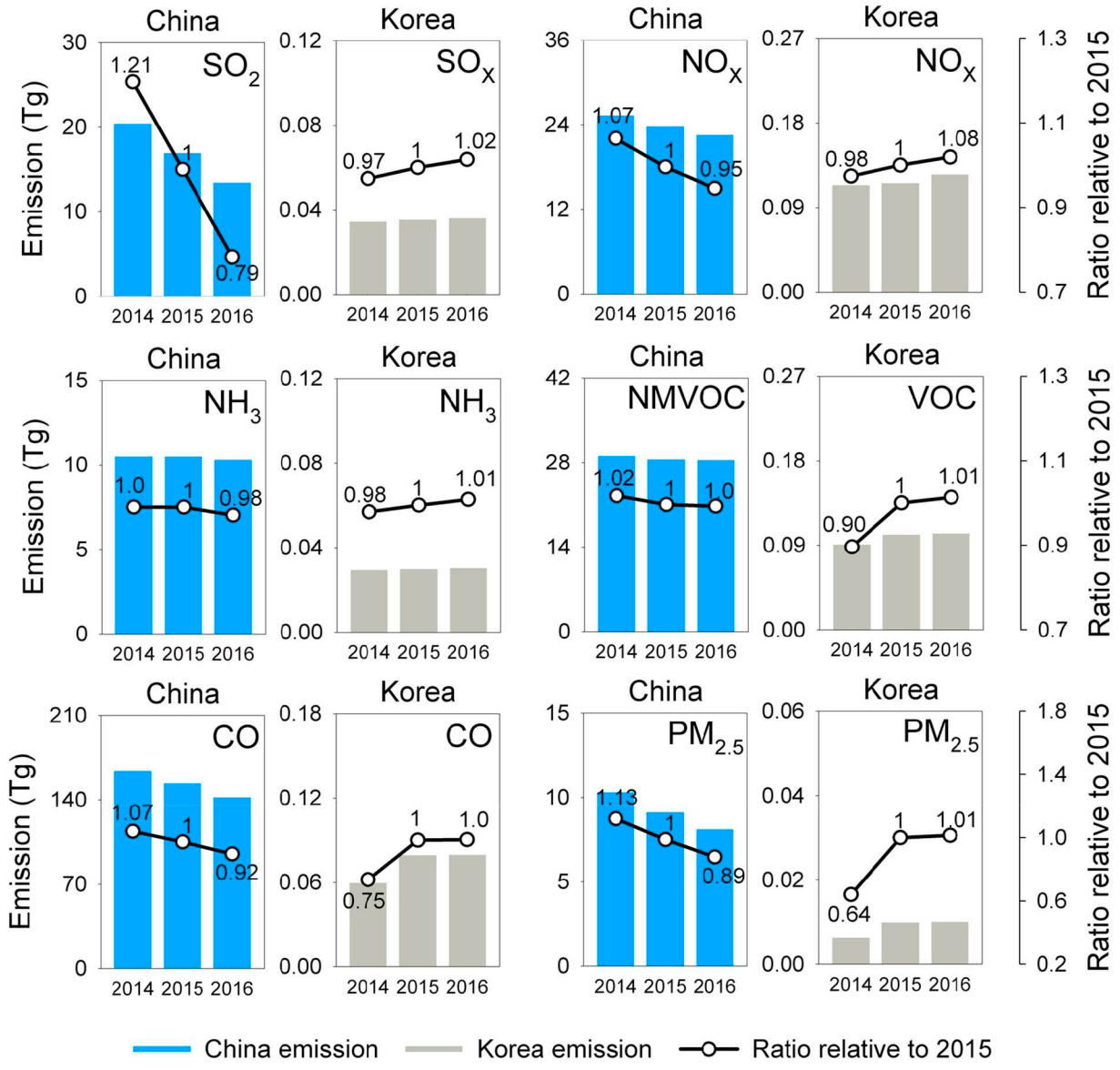

Fig. 2. Anthropogenic emissions in China and Korea from 2014 to 2016.

Despite these recent monitoring studies in China, there is little research on the changes in the response of chemical properties over background areas, or the plan's impact on the PM over the neighboring downstream areas over Northeast Asia. Changes in both the amount and chemical properties of the PM, especially at background aerosol monitoring sites, were expected to be ascribed to the second generation of

Table 1
Average concentrations (μg/m^3) of $PM_{2.5}$, non-sea-salt sulfate(nss-SO_4^{2-}), and nitrate(NO_3^-) observed at the Baengnyeong supersite with the standard deviation and maximum value (in brackets) and the ratio of sulfate to nitrate during "hazy" cases selected in this study. Asterisks(*) represent LRT cases, and *[1), 2)] and *[3)] denote representative LRT cases: LRT1, LRT2, and LRT3 selected for WRF-Chem simulations of 2014, 2015, and 2016, respectively.

Year	Case	Date	$PM_{2.5}$	nss-SO_4^{2-}	NO_3^-	Ratio (nss-SO_4^{2-} /NO_3^-)	LRT case
2014	1	03/08 14LST–03/09 10LST (21*h*)	47.0 ± 34.1 (136)	7.5 ± 5.9 (19.6)	3.4 ± 2.8 (10.5)	2.2	
	2	03/14 00LST–03/15 02LST (27 h)	64.6 ± 14.8 (88)	5.8 ± 1.9 (9.0)	1.9 ± 0.6 (2.9)	3.1	
	3	03/15 05LST–03/17 08LST (52 h)	61.2 ± 22.9 (99)	8.6 ± 1.9 (13.2)	4.0 ± 2.2 (8.9)	2.1	*[1)]
	4	03/18 07LST–03/20 05LST (47 h)	36.7 ± 18.6 (123)	3.6 ± 1.2 (6.6)	1.1 ± 0.5 (2.3)	3.3	*
	5	03/30 03LST–04/01 06LST (52 h)	50.1 ± 16.2 (97)	4.0 ± 1.8 (9.3)	1.5 ± 0.9 (5.5)	2.8	
	6	04/02 11LST–04/03 17LST (31*h*)	40.7 ± 12.5 (64)	5.9 ± 2.9 (11.4)	1.5 ± 1.5 (6.0)	4.1	
	7	04/09 10LST–04/11 01LST (40 h)	40.2 ± 7.2 (51)	11.4 ± 1.8 (15.8)	0.4 ± 0.1 (0.9)	27.6	
	8	04/18 09LST–04/21 02LST (66 h)	56.2 ± 13.6 (95)	4.3 ± 1.4 (7.6)	1.6 ± 0.6 (2.9)	2.8	
	9	04/22 16LST–04/25 18LST (75 h)	77.4 ± 32.5 (155)	17.0 ± 5.2 (27.7)	3.2 ± 2.1 (9.7)	5.3	*
	10	05/11 15LST–05/15 02LST (84 h)	61.0 ± 14.7 (87)	9.4 ± 4.2 (17.7)	5.1 ± 4.2 (19.4)	1.9	
2015	11	03/02 04LST–03/03 16LST (37 h)	55.7 ± 15.3 (88)	8.2 ± 3.2 (16.0)	5.3 ± 3.4 (13.2)	1.6	
	12	03/08 11LST–03/09 10LST (24 h)	37.4 ± 11.9 (63)	5.6 ± 1.5 (9.1)	5.5 ± 2.4 (9.6)	1.0	
	13	03/16 17LST–03/19 02LST (58 h)	49.8 ± 12.2 (74)	6.7 ± 2.2 (10.1)	6.7 ± 2.1 (9.3)	1.0	
	14	03/19 13LST–03/20 05LST (17 h)	74.6 ± 24.0 (106)	6.7 ± 0.8 (7.9)	15.7 ± 8.0 (26.0)	0.4	*
	15	03/21 02LST–03/22 05LST (28 h)	133.9 ± 46.1 (240)	14.1 ± 5.3 (22.2)	30.0 ± 13.4 (51.2)	0.5	
	16	04/12 06LST–04/13 01LST (20*h*)	38.6 ± 5.3 (47)	9.3 ± 1.6 (12.0)	4.4 ± 1.8 (9.2)	2.1	
	17	04/15 11LST–04/16 11LST (25 h)	61.9 ± 14.3 (82)	10.6 ± 1.9 (13.0)	10.9 ± 4.2 (16.9)	1.0	
	18	04/21 10LST–04/24 08LST (71 h)	53.2 ± 19.8 (96)	8.2 ± 3.4 (14.5)	9.5 ± 4.5 (22.5)	0.9	*[2)]
	19	04/25 13LST–04/27 08LST (44 h)	53.6 ± 17.8 (91)	11.4 ± 3.6 (20.0)	5.8 ± 3.8 (15.1)	2.0	
	20	05/14 11LST–05/15 14LST (28 h)	41.4 ± 6.6 (57)	5.7 ± 0.9 (7.3)	3.7 ± 1.3 (6.8)	1.6	
2016	21	03/04 08LST–03/04 20LST (13*h*)	37.8 ± 15.0 (57)	3.4 ± 1.5 (5.9)	6.0 ± 4.2 (14.4)	0.6	
	22	03/05 22LST–03/06 18LST (21 h)	89.5 ± 56.2 (228)	2.2 ± 0.3 (2.8)	0.7 ± 0.4 (1.9)	3.1	
	23	03/12 13LST–03/14 15LST (51 h)	48.3 ± 15.4 (72)	7.1 ± 2.1 (12.7)	6.8 ± 3.3 (13.3)	1.0	*
	24	03/21 19LST–03/22 22LST (28 h)	61.0 ± 12.7 (79)	4.4 ± 1.4 (8.0)	8.1 ± 2.4 (11.8)	0.5	*[3)]
	25	03/25 10LST–03/26 23LST (38 h)	36.2 ± 9.0 (55)	2.4 ± 0.7 (3.6)	5.0 ± 2.4 (10.6)	0.5	
	26	03/27 01LST–03/28 05LST (29 h)	41.2 ± 8.2 (58)	4.9 ± 0.8 (6.3)	9.8 ± 3.7 (19.9)	0.5	
	27	03/28 09LST–03/30 03LST (43 h)	58.1 ± 14.4 (84)	8.9 ± 2.4 (13.1)	9.9 ± 3.9 (16.4)	0.9	
	28	04/05 10LST–04/06 21LST (36 h)	38.5 ± 16.8 (90)	4.5 ± 1.8 (10.0)	9.0 ± 3.9 (17.9)	0.5	
	29	04/07 21LST–04/09 05LST (33*h*)	43.2 ± 16.1 (72)	7.1 ± 2.4 (13.2)	8.3 ± 5.6 (21.8)	0.9	
	30	05/25 08LST–05/26 10LST (27 h)	61.5 ± 14.2 (99)	14.0 ± 4.3 (20.3)	10.5 ± 6.1 (27.7)	1.3	

PM. Nevertheless, secondary chemical aerosol formations during the long-range transport (LRT) process and the general chemical composition of PM during the Chinese PCAP emission-control period are significant indicators of the impact of the changing emissions over Northeast Asia. Additionally, little attention has been paid to the factors determining the neutralization of acidity. Therefore, it would be vital to diagnose the acidity of the background atmosphere in response to the recent changes in Chinese emissions.

PM is made up of a complex mixture of organic and inorganic substances. Sulfate, nitrate, and ammonium are the leading Secondary Inorganic Aerosol (SIA) components in $PM_{2.5}$, mainly occurring as ammonium sulfate ($(NH_4)_2SO_4$) and ammonium nitrate (NH_4NO_3), which are the products of the neutralization of sulfuric acid (H_2SO_4) and nitric acid (HNO_3), respectively, with ammonia (Stockwell et al., 2003; Squizzato et al., 2013). Previous studies have reported that sulfate, nitrate, and ammonium in Seoul, Capital of South Korea, accounted for 30 to 50% of $PM_{2.5}$ mass concentration (Han and Kim, 2015; Kang et al., 2004; Kang et al., 2006; Kim, 2006; Kim et al., 2007; Shon et al., 2012) and elevated SIA components contribute significantly to the formation of extensive $PM_{2.5}$ pollution in China (Guo et al., 2014; Huang et al., 2014; Tao et al., 2017; Tian et al., 2017; Tian et al., 2019; Wang et al., 2016a). More recent data have suggested that sulfate has decreased, accompanied with increasing nitrate, compared to earlier years, and consistent with the trends of their respective gaseous precursors emissions (Tian et al., 2017; Tian et al., 2019; Wang et al., 2017; Yang et al., 2011), and high nitrate contributions were reported during several haze episodes in China (Li et al., 2018; Tian et al., 2017; Yang et al., 2017). The relative contributions of the chief secondary inorganic aerosols to severe $PM_{2.5}$ pollutants may have changed in recent years in China (Tian et al., 2019), but the causes and persuasive interpretations for the reported features during the LRT process are still lacking.

The government of South Korea manages a national air quality forecast system of comprehensive monitoring sites for particulate matter (PM_{10}, $PM_{2.5}$), and the Baengnyeong (island) supersite is designed to monitor the regional background concentration and long-range transboundary air pollutants (NIER, 2015; NIER, 2017).

The primary objective of this study is to diagnose the trends of the inorganic composition of particulate matter at the Baengnyeong supersite from 2014 to 2016 to interpret the impact of the evolutional sulfur reduction in the Chinese anthropogenic emission sources on regional background areas. The study focused on the spring season, which yields the highest PM levels in Korea with the higher LRT frequencies. The study used the ground-based measurements from the Baengnyeong supersite, which is one of the representative background areas located between China and Korea (Lee et al., 2015).

Additionally, the WRF-Chem model (the Weather Research and Forecasting (WRF) model coupled with Chemistry) was employed to investigate the impacts of the Chinese emissions reduction on contributing to the inorganic aerosol components such as sulfate, nitrate, and ammonium over the downstream area of China. Also changes in both the chemical compositions and the aerosol acidity of the regional background area in Northeast Asia were investigated by using the combined results of the in-situ measurements and the modeling results.

2. Method and data

2.1. Observation site, ionic species, and instruments

The regional background observation site, the Baengnyeong supersite (37°57′52.9″N, 124°38′02.4″E) (referred to as "B-site") is indicated in Fig. 1. B-site is located in the Yellow Sea, west of the Korean Peninsula, and is situated approximately 180 km from the Chinese Shandong Peninsula, and is deemed suitable for monitoring the impact of long-range transported air pollutants from a variety of source regions such as Eastern China. The inorganic species measured at B-site were sulfate, nitrate, and ammonium components. Ammonium in PM exists

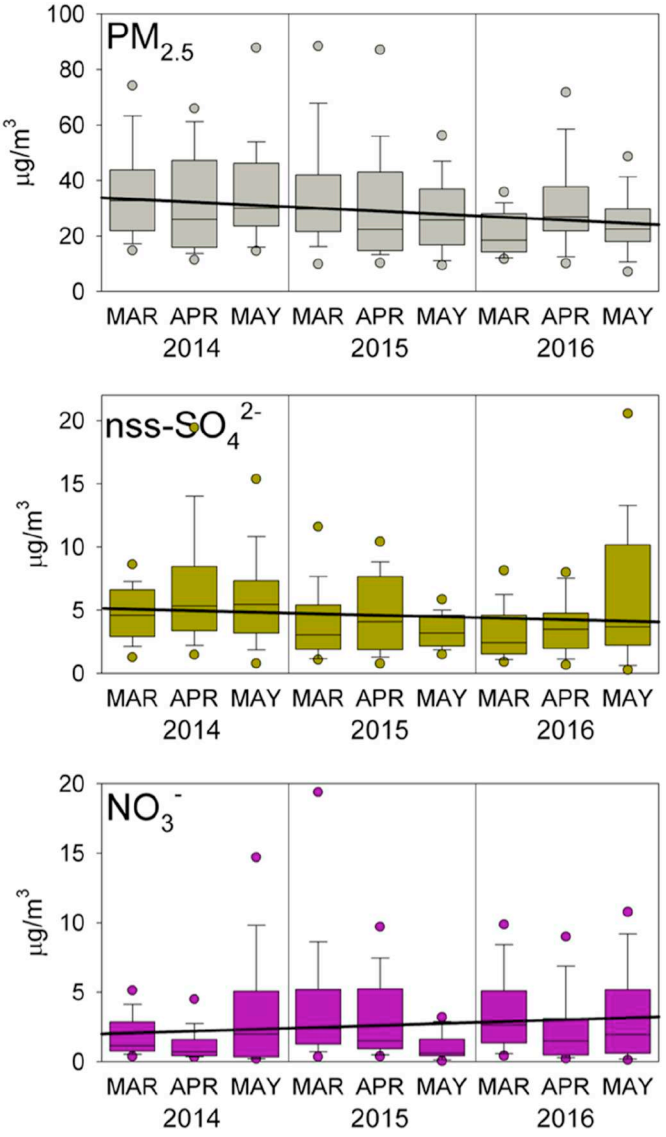

Fig. 3. Annual trends of spring $PM_{2.5}$, non-sea-salt sulfate (nss-SO_4^{2-}), and nitrate (NO_3^-) measured at Baengnyeong supersite. The black lines represent the linear regression line.

as ammonium sulfate and ammonium nitrate, and its concentration is dependent on sulfate and nitrate, respectively.

An ambient ion monitor (AIM, URG-9000D/USA) for the ionic species present in $PM_{2.5}$ was used at B-site (NIER, 2015). The AIM monitor drew air in through the $PM_{2.5}$ inlet at a controlled rate of 3 L/min to remove the large particles from the air stream (Park et al., 2013). The sample was then drawn through a membrane-type liquid diffusion denuder coated with 30% H_2O_2, where the interfering gaseous species were removed (Park et al., 2013). In order to achieve high collection efficiencies, the particle-laden air stream then entered the aerosol super-saturation steam chamber to enhance the particle growth (Park et al., 2013). The enlarged particles (i.e., droplets) were collected every hour by an inertial particle separator and were then injected into the ion chromatograph (IC) (Park et al., 2013).

In the current analysis of sulfate sampling, the amount of non sea salt sulfate (nss-SO_4^{2-}) was calculated by subtracting the SO_4^{2-} amount (Carmichael et al., 1997; Finlayson-Pitts and Hemminger, 2000; Ohta and Okita, 1990) in association with sea water from total measured particulate sulfate in $PM_{2.5}$ samples.

2.2. Model and emissions of 2014–2016 over Northeast Asia

The model, WRF-Chem (ver. 3.8.1), is an online-coupled meteorology-chemistry-aerosol model, which simultaneously simulates trace gases and aerosols with the WRF-derived meteorological fields. The meteorological model WRF is a fully compressible and non-hydrostatic mesoscale numerical weather prediction model (Skamarock and Klemp, 2008), and the air quality and meteorological components use the same advection, grid, and physics schemes for sub-grid scale transport (Fast et al., 2006; Grell et al., 2005).

In the current study, a suitable model domain and the horizontal resolution were established for the area over Northeast Asia. The horizontal resolution of 27 km × 27 km was applied in the study domain (Fig. 1), covering Northeast Asia (100°E–150°E longitude, 20°N–50°N latitude) with 174 (W–E) × 128 (S—N) grid points and 15 vertical layers (sigma levels). Initial and boundary conditions for the meteorological variables were obtained from 6-hourly 1° × 1° data from the National Centers for Environmental Prediction (NCEP) Final Analysis (FNL) data (NCEP, 2000). The WRF-Chem model has various chemical mechanisms available (Lee et al., 2019), and Table S1 summarizes the physical and chemical options for the WRF-Chem simulation.

As a basic emissions inventory, Comprehensive Regional Emissions inventory for Atmospheric Transport Experiment for the base year of 2015 (CREATE-2015) which was employed for anthropogenic emissions data for East Asia. CREATE-2015 is based on the Multi-resolution Emission Inventory of China (MEIC, http://www.meicmodel.org/), Clean Air Policy Support System (CAPSS, http://airemiss.nier.go.kr), and Regional Emission Inventory in Asia (REAS) version 2 (http://www.jamstec.go.jp/frsgc/research/d4/emission.htm) and is also used for both MAPS-Seoul (Megacity Air Pollution Studies-Seoul) and KORUS-AQ (Korea-US Air Quality)-2016 campaigns (Woo et al., 2014; Kim et al., 2018).

As this study focused on the tremendous emissions reduction period under PCAP and the subsequent three years (from 2014 to 2016), Chinese emissions from 2014 and 2016 were newly generated from both CREATE-2015 and the MEIC emissions (Zheng et al., 2018b). MEIC emissions reported the trends of Chinese anthropogenic emissions from 2010 to 2017 on a chemical species basis (Zheng et al., 2018b), and the total ratio of emissions in China from MEIC for each chemical species was calculated for both 2014 and 2016 relative to 2015. We applied these annual "scaling factors" to CREATE-2015, generated emissions for both 2014 and 2016 years. South Korean emissions were updated based on CAPSS data, and the data for other regions such as Mongolia and Southern Russia were taken from CREATE-2015 with no modifications.

The biogenic emissions were employed by using the Model of Emissions of Gases and Aerosols from Nature (MEGAN)(version 2) emission module (Guenther et al., 2006). Sea salt emissions and biomass burning emissions were both considered from the FINN model in the WRF-Chem model. MEGAN has been fully coupled into WRF-Chem to enable the online calculation of biogenic precursor emissions and was subject to vegetation cover and meteorological conditions such as temperature and solar radiation at the time of the calculation (Grell et al., 2005).

Fig. 2 shows the annual trends of emissions for the three years (2014–2016) employed in this study. As noted in Fig. 2, SO_2 and NOx emissions in 2016 had fallen by 34% and 11%, respectively, since 2014, and NH_3 emissions had fallen by 1.9%, indicating almost no inter-annual change over the three years. The SO_2/NO_x emission ratios for emissions from 2014 to 2016 in China were 0.81, 0.71, and 0.60, respectively, which had decreased by approximately 26% since 2014, implying the change into nitrate-favored formation of the secondary inorganic aerosols.

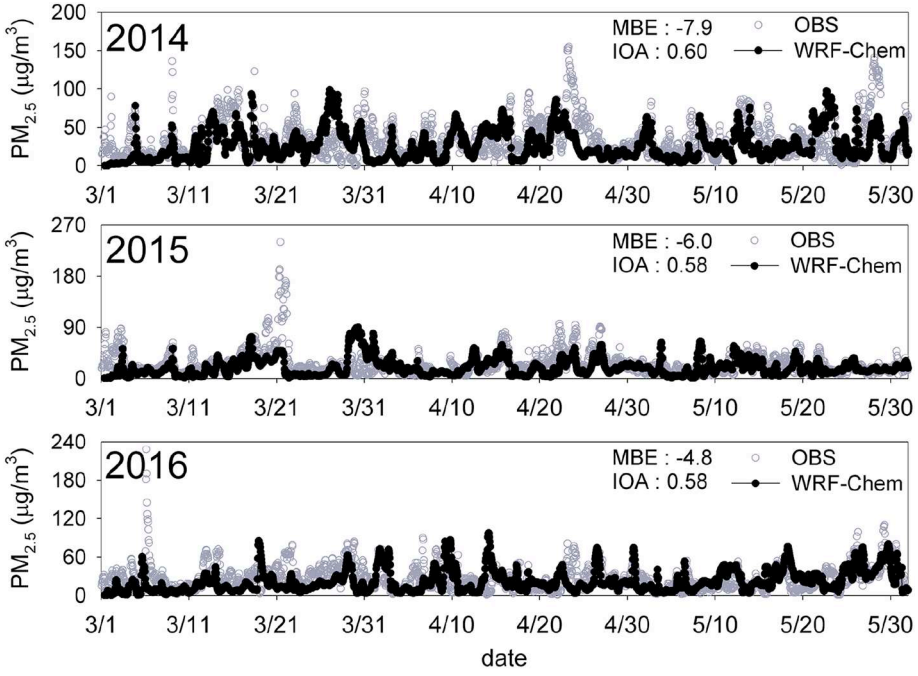

Fig. 4. Timeseries of hourly observed (gray dot) and simulated (black dot) $PM_{2.5}$ mass concentrations at the Baengnyeong supersite in spring during 2014–2016.

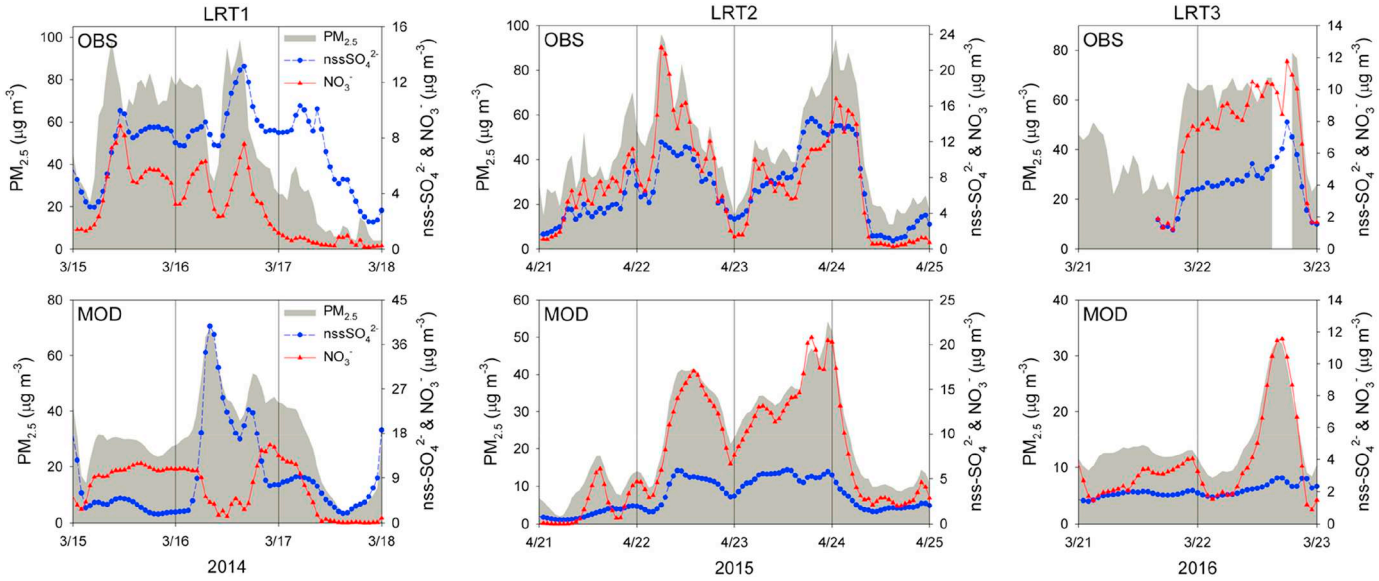

Fig. 5. Timeseries of observed and simulated $PM_{2.5}$, non-sea-salt sulfate ($nss\text{-}SO_4^{2-}$) and nitrate (NO_3^-) during the selected LRT cases.

2.3. Case selection

According to the monthly average concentrations of the inorganic species in Korea, nitrate was predominant in February, March, and April because, nitrate in the fine mode tends to be volatile under high-temperature conditions (Hassan et al., 2013; Matsumoto and Tanaka, 1996), whereas, sulfate generally was predominant in February, April, and July. With this background, the spring seasons from 2014 to 2016 were selected as the study period because both sulfate and nitrate are high.

Table S2 summarizes the average concentrations of $PM_{2.5}$, sulfate, and nitrate observed at B-site during the spring seasons of 2014 to 2016. As the first step in case selection, the study defined a springtime "hazy" case as a period showing considerable $PM_{2.5}$ levels at B-site, with the observed average concentration greater than the air quality standard (35 μg/m^3) for $PM_{2.5}$ in South Korea. Among the selected hazy cases (Table 1), LRT-dominant cases were selected as per Jo and Kim. (2013), based on synoptic weather charts and air-mass trajectories (Fig. S1 and S2). The synoptic weather charts and the meteorological data were all obtained from the Korea Meteorological Administration (KMA) in this study.

As an air-mass trajectory model, HYSPLIT–4 (Hybrid Single-Particle Lagrangian Integrated Trajectory; Draxler, 1999; Draxler and Rolph, 2012; Rolph et al., 2017; Stein et al., 2015; https://ready.arl.noaa.gov/HYSPLIT_traj.php) was utilized to compute the air pollution trajectories for the selected LRT cases. In this study, the HYSPLIT-4 model was employed to track the moving air masses during the computed 6-day trajectories (3 days backward and 3 days forward from the selected day) for the LRT case selection. For example, during the six consecutive days, the case where both "pre-3 day backward" and "post-3 day

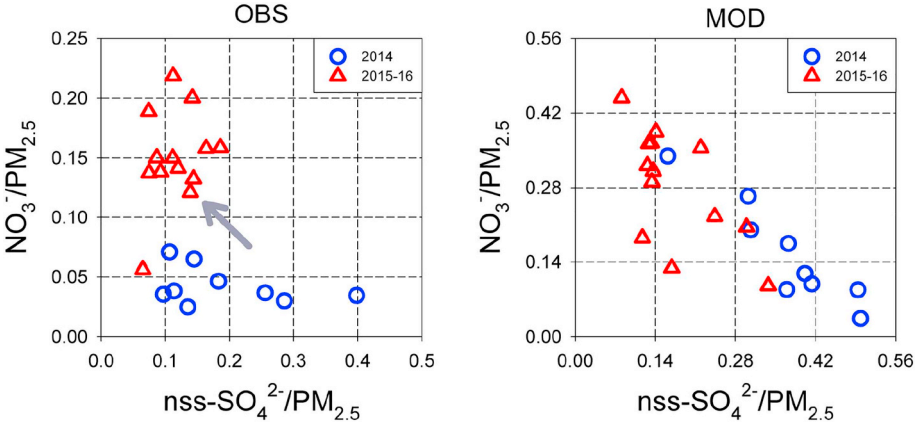

Fig. 6. Scatter diagram of the ratio of non-sea-salt sulfate (nss-SO_4^{2-}) to $PM_{2.5}$ and nitrate (NO_3^-) to $PM_{2.5}$ during LRT days in 2014 (blue circle) and in 2015–2016 (red triangle), respectively. (For interpretation of the references to colour in this figure legend, the reader is referred to the web version of this article.)

forward" trajectories remained within the defined inner box was designated as a non-LRT case (see Jo and Kim, 2013). Otherwise, the result was designated as an LRT case (Fig. S1).

As a result, a total of 30 hazy cases were selected for the study period, and the detailed chemical results of measurements were analyzed (Table 1). The results were further refined, and seven representative LRT cases were selected as detailed case studies in the model simulations: three cases in 2014, two cases in 2015, and two cases in 2016 (also listed in Table 1). The seven selected representative LRT cases incurred wind fields of mostly westerly, southwesterly, and northerly winds prevailing in western coastal area, allowing the air pollutants to be transported from China to the Korean Peninsula.

3. Results

3.1. Observed annual trends of springtime nitrate and sulfate

Table S2 shows annual mean $PM_{2.5}$, sulfate, and nitrate concentrations. As indicated in Table S2 the averages of sulfate and nitrate observed at B-site in spring 2014, were 5.7 and 2.1 μg/m^3, respectively, indicating that sulfate was generally higher than nitrate in 2014. However, as sulfate showed a small decrease, nitrate had significantly increased by 30% (2.7 μg/m^3) in 2015 and 48% (3.1 μg/m^3) in 2016, compared with 2014, denoting the considerable increase of nitrate (see Table S2).

Table 1 summarized $PM_{2.5}$, sulfate, nitrate, and sulfate/nitrate (S/N) ratios for all 'hazy' cases. The asterisks denoted in Table 1 represent the seven representative LRT cases during the study period. The observed (S/N) ratios during the hazy cases ranged from 1.9–27.6 in 2014. However, (S/N) ratios ranged from 0.4–2.1 in 2015, and 0.5–3.1 in 2016 during the hazy cases. As a result, the concentration differences ($\triangle C = C_{sulfate} - C_{nitrate}$) between two sulfate and nitrate had decreased from 3.6 to 1.2 μg/m^3 from 2014 to 2016 (see Table S2), denoting again that the sulfate dominance in 2014 was clearly reduced, whereas nitrate became significant for the two years:2015 and 2016.

The inter-annual trends from 2014 to 2016 (Fig. 3) reiterated that the annual trend of $PM_{2.5}$ slowly declined, and sulfate was declining, as previously mentioned. Whereas, nitrate had steadily increased over the period, reiterating that the relative contribution of nitrate to the $PM_{2.5}$ mass concentrations was clearly on the rise throughout the study period (2014–2016). It is suggesting again that the change in the (SO_2/NO_x) emissions ratios may have been incorporated into the secondary chemical composition via complicated SIA formation pathways in the atmosphere over Northeast Asia.

3.2. Modeling and interpretation of inter-annual trends of inorganic species

Fig. 4 shows a time series of hourly $PM_{2.5}$ concentrations simulated by WRF-Chem against observations. WRF-Chem showed general features with no significant biases: Mean Bias Error (MBE) of −7.9 and Index of Agreement (IOA) of 0.6 in 2014. Only a few exceptional cases of overestimations (i.e., Mar/27 – Mar/28), and underestimation (i.e., Apr/23) in 2014, were noted. In 2015 and 2016, the model also showed features and general peaks with MBEs of −6.0 and − 4.8 in 2015 and 2016, respectively, and IOAs of 0.58 for both 2015 and 2016, except for some underestimation periods such as Mar/21 in 2015 and Mar/6 in 2016.

Fig. 5 shows the time series of the three representative LRT cases listed in Table 1: Mar/15–17/2014 (LRT 1), Apr/21–24/2015 (LRT 2), and Mar/21–22/2016 (LRT 3). The results for the LRT 1 case show that $PM_{2.5}$ concentrations started to increase at 0700 LST on March 15 and continued to rise until 1500 LST on March 16, reaching the maximum concentration of 99 μg/m^3, primarily contributed by sulfate. However, LRT 2 and LRT 3 showed one or two peaks, with nitrate as the leading contributor (e.g., 0600 LST on April 22 and 0100 LST on April 24 (for LRT 2), and 1900 LST on March 22 (for LRT 3)). Two cases: LRT 2 (2015) and LRT 3 (2016), indicated a considerable dominance of nitrate for both the observations and simulations.

Fig. 6 shows a scatter diagram of the ratio of SO_4^{2-} to $PM_{2.5}$ and NO_3^- to $PM_{2.5}$ for the seven hazy LRT cases (denoted with asterisks in Table 1). The (S/N) ratios overall were higher in 2014, at 5.5 ± 7.8 (mean ± standard dev.) with a maximum of 27.6 (Table 1 and Fig. 6). These values are significantly different from the values observed in Korean urban areas: nitrate in Seoul, Capital of South Korea, was much more dominant than sulfate with higher maximum concentrations by a factor of 2.2, 2.1, and 1.4, respectively, contrasting the results from B-site. In contrast to 2014, however, the (S/N) ratios in 2015–2016 yielded different distributions, as listed in Table 1. The (S/N) ratios in 2015 showed 1.2 ± 0.6 (mean ± standard dev.) with the maximum of 2.1, and in 2016, it showed 1.0 ± 0.8 (mean ± standard dev.) with the maximum of 3.1 (Table 1), showing strong nitrate dominances for the two years, presumably due to the anthropogenic secondary inorganic aerosol formations. This tendency is also apparent in Fig. 6, where sulfate and nitrate accounted for 9.7 to 39.8% and 2.5 to 7.1% of the $PM_{2.5}$ mass concentration, respectively, in 2014. Whereas, in 2015 and 2016, sulfate and nitrate accounted for 6.5 to 18.6% and 5.6 to 21.9% of the $PM_{2.5}$ mass concentration, respectively, reiterating the distinct increase in the contribution of nitrate to the high $PM_{2.5}$ concentrations in latter two years.

This study suggests ubiquitous increases in nitrate and decreases in sulfate under favorable LRT conditions in 2015 and 2016, compared to 2014, presumably as a chemical response to the rapid sulfur reduction

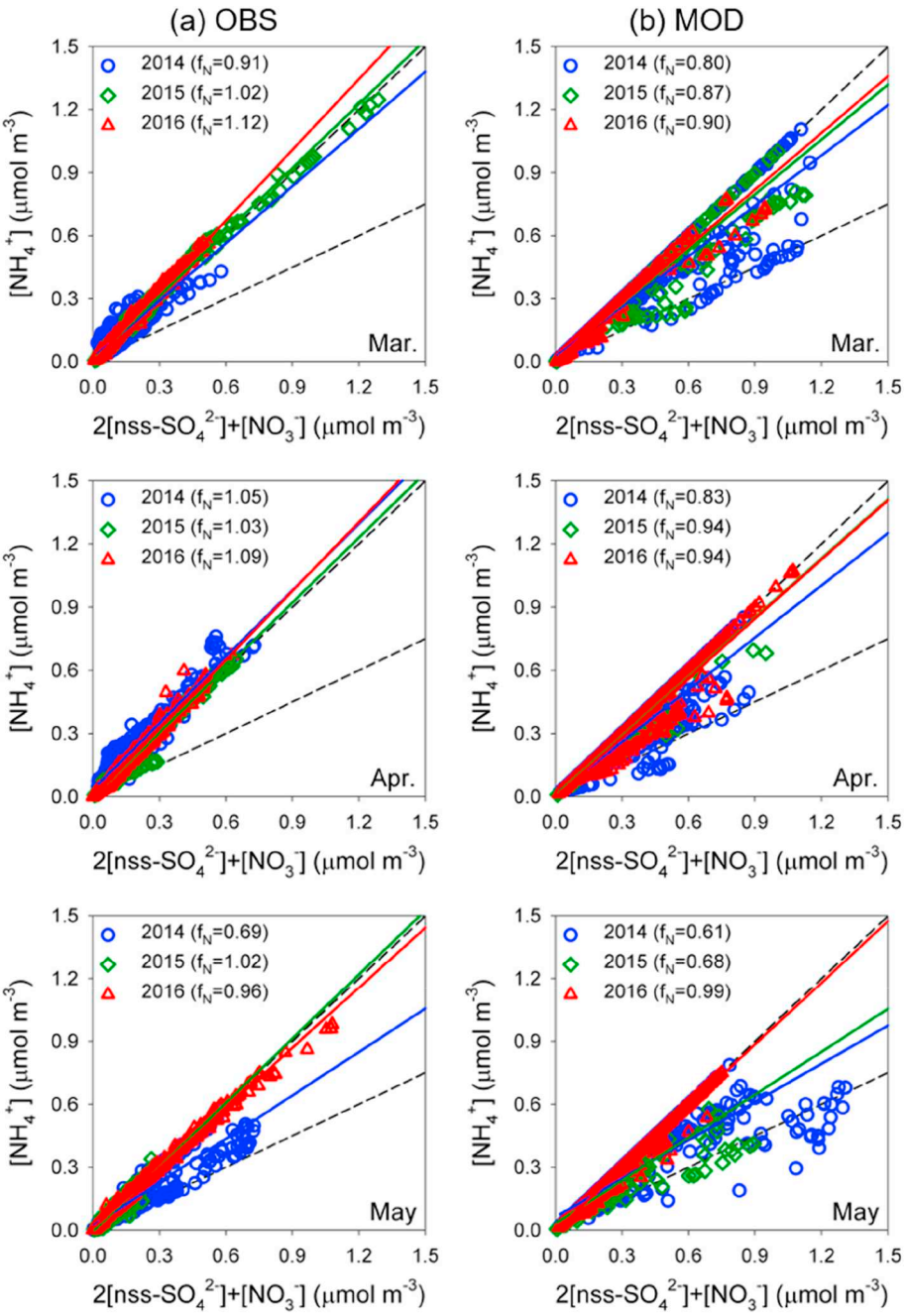

Fig. 7. Scatter plots of (a) observed and (b) simulated acid aerosol neutralization in March, April, and May, as given by the [NH_4^+] versus 2[nss-SO_4^{2-}] + [NO_3^-] relationship.

through the Chinese air action of PCAP initiated in 2013.

3.3. Acidity of the aerosol and its annual trends over Northeast Asia

To diagnose the changing aerosol acidity over Yellow Sea Area, the neutralization parameter, f_N (=[NH_4^+]/ (2[SO_4^{2-}] + [NO_3^-])) was employed here for convenience. The study used f_N, is the same as *f*, the neutralization parameter, used by Zhang et al. (2007) and Fisher et al. (2011). The parameter *f* was reconstructed into f_N (the slope of anion vs. cation by switching the x- and y-axis) on the same *f*-space, to indicate the larger f_N toward greater neutralization. Here, f_N = 1 implies an $(NH_4)_2SO_4$ sulfate aerosol (solid or aqueous), while f_N = 0.5 indicates an NH_4HSO_4 sulfate aerosol in bulk (Fisher et al., 2011; Zhang et al., 2007). All concentrations associated with f_N are given in molar units. It is recognized that observations with f_N > 0.9 means that sulfate was neutralized, whereas f_N > 1 (excess aerosol ammonium) could not be reconciled with sulfate-nitrate-ammonium aerosol thermodynamics, except for the case of the neutralization of organic acids with ammonia (e.g., Dinar et al., 2008; Mensah et al., 2011).

Fig. S3 shows the schematic diagram of f_N, illustrating the aerosol neutralization regimes on f_N –space, and Fig. 7 shows the distributions of f_N for both observations and simulations over three years. Fig. 7 (left panel) indicates that the observed aerosol acidity had been changing at a slower pace in March, with the f_N of 0.91, 1.02, and 1.12 for 2014, 2015, and 2016, respectively, explored the aerosol acidity toward neutralization. In April, the change in f_N was not dominant, with the f_N of 1.05, 1.03, and 1.09 for 2014, 2015, and 2016, respectively. However, in May, f_N shows 0.69, 1.02, and 0.96 for 2014, 2015, and 2016, indicating relatively more acidic conditions in 2014 and changing toward neutralized aerosols in 2015 and 2016.

Table 2
Inter-annual variations of three SIA (Secondary Inorganic Aerosol) formation parameters: neutralization fraction of aerosol (f_N), degree of sulfate neutralization (DSN), and adjusted gas ratio (AGR); simulation by the WRF-Chem model.

	Year	Spring	March	April	May
	f_N (Neutralization Parameter, Zhang et al., 2007)				
Observation	2014	0.84	0.91	1.05	0.69
	2015	1.03	1.02	1.03	1.02
	2016	1.01	1.12	1.09	0.96
Simulation	2014	0.74	0.80	0.83	0.61
	2015	0.85	0.87	0.94	0.68
	2016	0.95	0.90	0.94	0.99
	DSN (Degree of Sulfate Neutralization, Pinder et al., 2008)				
Observation	2014	1.83	1.84	2.13	1.18
	2015	2.04	2.12	2.01	1.92
	2016	1.96	2.40	2.19	1.85
Simulation	2014	1.33	1.50	1.45	1.05
	2015	1.56	1.67	1.73	1.23
	2016	1.79	1.70	1.79	1.87
	AGR (Adjusted Gas Ratio, Wang et al., 2016b)				
Observation	2014	N/A	N/A	N/A	N/A
	2015	N/A	N/A	N/A	N/A
	2016	N/A	N/A	N/A	N/A
Simulation	2014	0.62	0.86	0.75	0.47
	2015	0.78	0.75	0.91	0.51
	2016	0.79	1.08	0.82	0.76

In the WRF-Chem model, as indicated in Fig. 7 (right panel), the simulated f_N was simulated with the predominant changes in aerosol acidity over the years. The simulated aerosol in March in 2014 was acidic, with the f_N of 0.80, and steadily changed to a more neutralized aerosol with the f_N of 0.87 and 0.90 in 2015 and 2016. In April, the model simulated the gradual change in acidity toward neutralization with the f_N of 0.83 (2014), 0.94 (2015), and 0.94 (2016), respectively, showing slight change to neutralization annually. In May, the f_N shows 0.61, 0.68, and 0.99 for the three years, indicating acidic aerosol in both 2014 and 2015, but jumps toward neutralization in 2016. Overall, WRF-Chem model simulations also showed similar trends to observations, although the model slightly underestimates the neutralization for all three months.

4. Discussion

SO_2 is recognized to be a more substantial transboundary air pollutant over Northeast Asia in the 1990s and 2000s (Carmichael et al., 2002; Kim et al., 2001; Park and Lee, 2003; Wang et al., 2008). Generally, sulfate can be transported further than nitrate because nitrogen-related atmospheric chemistry is more active than that of SO_2 (Zhang et al., 2012), and thus, sulfate has a longer atmospheric lifetime (1–2 weeks) than nitrate (Lin et al., 2008), and sulfur takes more time to be fully neutralized than nitrogen. On the other hand, Lin et al. (2008) discussed the roles of NOx emissions emitted from transportation sources in Japan and South Korea and suggested the significant local contribution from nitrogen (Lin et al., 2008; Streets et al., 2013). Relatively strong local NOx emissions periodically led to local contributions to nitrate, resulting in higher levels than sulfate.

The observed concentration differences between sulfate, nitrate, and their ratios may be attributable to their ability of neutralization in Northeast Asia, depending on 'ammonia-poor' or 'ammonia-rich' conditions, and 'SO_2-poor condition' in China due to the decrease in the (SO_2/NO_x) emissions ratios provide further insight into nitrate peaks over Yellow Sea area.

Together with f_N, we introduced two more indicators: the degree of sulfate neutralization (DSN) and "adjusted" gas ratio (AGR), as employed by Pinder et al. (2008) and Wang et al. (2016b). DSN and AGR were defined as DSN = ($[NH_4^+]$ - $[NO_3^-]$)/$[SO_4^{2-}]$, and AGR = ($[NH_3]$ + $[NO_3^-]$)/($[HNO_3]$ + $[NO_3^-]$), respectively. Here, DSN was an estimate of the degree of sulfate neutralization by ammonium, and is a similar indicator to f_N, as discussed in Section 3.3. DSN has 3 degrees of sulfate neutralization; 1) DSN = 1 sulfate exists as ammonium bisulfate (Dennis et al., 2008), 2) 1 < DSN < 2, there is a coexistence of sulfate and bi-sulfate (Chang et al., 2018), and 3) DSN > 2, there is sufficient ammonium to fully neutralize the sulfuric acid (Wang et al., 2016b). Alternatively, AGR, the "adjusted" gas ratio of free ammonia to total nitrate introduced by Pinder et al. (2008), could be used as an indicator of aerosol nitrate sensitivity to the change in three emissions: NH_3, SO_2, and NOx (Wang et al., 2016b). For example, AGR less than 1 is an "ammonia-poor" condition, and nitrate can be increased, replacing the decreased sulfate. With an abundance of free ammonia, AGR should be greater than 1 ("ammonia-rich" condition), and nitrate is sensitive to the changes in the total nitrate (= $[HNO_3]$ + $[NO_3^-]$) (Dennis et al., 2008). When AGR is approaching 1, the SIA formation is in transition regime between the non-replacement and replacement regimes, and a nitrate response to the sulfate emissions reduction is expected (Dennis et al., 2008; Pinder et al., 2008).

Table 2 shows the summary of three indicators: f_N, DSN, and AGR for both the observations and simulations at B-site. The DSN shows similar trends to f_N over the study period. Observations showed a slow increase of DSN from 1.83 (2014) to 2.04 and 1.96 (2015 and 2016, respectively) with a sharp increase in May in particular. WRF-Chem also indicated small increasing trends from 1.33 (2014) to 1.56 and 1.79 (2015 and 2016, respectively), reiterating a similar increasing trend to f_N, as listed in Table 2 and Fig. 7. This trend suggests that f_N > 1 in 2015, indicating that sulfate was fully neutralized in 2015, whereas the modeled f_N was approaching 1 from 2014 to 2016. In comparison to 2014, the results show a nitrate-increase and sulfate-decrease at B-site in 2015 and 2016, denoting that sulfate had been reduced entirely, directly due to the SO_2-poor condition caused by PCAP's sulfur reduction.

AGR also shows increasing inter-annual trend with the AGR < 1, but approaching 1 (Table 2). The AGRs were determined from modeling only because of the lack of adequate or quantitative measurements of the HNO_3 and NH_3 species. The simulated AGR shows an overall steady increase from 0.62 (2014) to 0.78 and 0.79 (2015 and 2016, respectively) in Spring (Table 2). In previous studies, the AGR was generally higher than 1 over most inland areas, and less than 1 over marine areas over Northeast Asia (Wang et al., 2016b). In this study, AGR < 1 was found at B-site. Therefore, the WRF-Chem simulations with the AGR < 1 (= 0.62–0.79) corresponds to the results of Wang et al. (2016b), considering that B-site (Fig. 1) is background site located in the Yellow Sea (marine area).

The increasing AGR approaching 1 indicates the transition from SO_2-rich to SO_2-poor conditions, suggesting that nitrate would not directly respond to the reduction of SO_2 emissions in 2014. However, in 2015 and 2016, the modeling results of AGR approaching 1 signifies that the ammonia response to SO_2-poor condition (i.e., DSN > 1 in Table 2), but still had a limited capacity to fully form nitrate as AGR approaches 1: the transition occurred from SO_2-rich to SO_2-poor condition over the study period. The abundant SO_2 emission and its incompletion of neutralization in SO_2–rich condition in 2014 was evidenced by high proportion of both gaseous sulfur and nitric acid (DSNs < 2 and AGR < 1 in 2014), signifying that the amount of SO_2 was sufficient and needed more time to be fully neutralized even though Beijing and surrounding areas are characterized by high concentration levels of atmospheric NH_3. However, as atmospheric condition had become relatively more SO_2-poor condition in 2015, SO_2 became fully neutralized (DSN > 2 and AGR~1 in Table 2) in response to the SO_2 emission reduction. Ammonia was nevertheless sufficient in China to neutralize particulate sulfate and nitrate in Beijing (i.e., AGR~1) through the study period, more active nitrate formation occurred in SO_2-poor condition in 2015 and 2016, compared with that in SO_2-rich condition in 2014.

Ammonia emissions, which are currently one of the most important model inputs, are mainly originating from agricultural sectors. Ammonia measurement data is also not available over Northeast Asia, especially over Yellow Sea. Therefore, the role of ammonia in the Yellow Sea should be identified from the detailed measurements in association with the long-range transport process over the marine atmosphere. In this study, we employed both model results mainly and limited measurements: additional modeling and comprehensive observational studies would be necessary to improve the understanding of nitrate and SIA formation mechanisms under various atmospheric SIA conditions. More recently, data from the April 2016 KORUS-AQ aircraft campaigns based in South Korea and the Yellow Sea could provide unprecedented information on the vertical distribution of sulfate-ammonium aerosols throughout the depth of the boundary layer in Northeast Asia. The current study will continue using the same KORUS-AQ data sets observed as well as WRF-Chem to investigate the implications for aerosol acidity over Northeast Asia.

5. Summary and conclusion

The primary objectives in this study are to understand the Chinese emissions reduction and its contribution to the formation of sulfate, nitrate, ammonium, and aerosol acidity in the atmosphere over the regional background area in Northeast Asia. We employed measurements at Baengnyeong supersite, a representative regional background site, and investigated the annual trends of springtime sulfate and nitrate during the high PM events in spring 2014–2016.

The results indicated that nitrate observed at Baengnyeong site had been clearly on the rise, whereas sulfate and $PM_{2.5}$ concentrations were on the decline. In spring 2014, sulfate was generally higher than those of nitrate. On the contrary, in 2015 and 2016, nitrate had increased by 30% (in 2015) and 48% (in 2016) compared to 2014, whereas sulfate had decreased. The ratio of the inorganic species to $PM_{2.5}$ for all days in the LRT cases showed distinct changes in the aerosol chemical compositions: a decrease in sulfate and increase in nitrate from 2014 to 2016.

We also see that the observed and modeled aerosol acidity were both changing at a slower pace over the same area with the neutralization parameters, and the results are indicating relatively more acidic conditions in 2014 and then shifting to neutralization in 2015 and 2016. WRF-Chem model diagnosed the neutralization based on the SIA formation, and indicated that the large amount of SO_2 in 2014 should be primarily responsible for the high proportion of both gaseous sulfur and nitric acid, and thus, the amount of SO_2 was not sufficient to be neutralized. In 2015 and 2016, however, sulfur was fully neutralized as sulfur emissions were reduced rapidly, and therefore, nitrate had begun to increase in response to the SO_2 reduction, and the nitrate had begun in SO_2-poor condition during the study period of 2015 to 2016.

However, a detailed analysis would be hampered by lack of observation of chemical species such as ammonia and nitric acid. Therefore, additional modeling and observational studies are necessary to improve the understanding of inorganic SIA chemical reactions under various atmospheric conditions. In this regard, the comprehensive aircraft campaign such as the KORUS-AQ Campaign will be beneficial to aid in the collection of the species relevant to the sulfate-nitrate-ammonium aerosols. Further study will continue using the KORUS-AQ Campaign data to investigate the impact of Chinese emissions mitigation and to quantify aerosol acidity over the regional background areas in Northeast Asia.

Declaration of Competing Interest

The authors declare that they have no known competing financial interests or personal relationships that could have appeared to influence the work reported in this paper.

Acknowledgements

This work was partially supported by the Grant (No. NIER-RP2016-182) from the research program of National Institute of Envirnmental Research (NIER), and partially supported by the Grant (No. NRF-2019R1I1A1A01060445). Also thanks are given to the anonymous reviewers for their helpful comments.

Appendix A. Supplementary data

Supplementary data to this article can be found online at https://doi.org/10.1016/j.atmosres.2020.104948.

References

Carmichael, G.R., Hong, M.S., Ueda, H., Chen, L.L., Murano, K., Park, J.K., Lee, H., Kim, Y., Kang, C., Shim, S., 1997. Aerosol composition at Cheju Island. Korea. J. Geophys. Res. 102, 6047–6061.

Carmichael, G.R., Calori, G., Hayami, H., Uno, I., Cho, S.Y., Engardt, M., Kim, S.B., Ichikawa, Y., Ikeda, Y., Woo, J.H., Ueda, H., Amann, M., 2002. The MICS-Asia study: Model intercomparison of long-range transport and sulfur deposition in East Asia. Atmos. Environ. 36, 175–199.

Chang, W., Zhan, J., Zhang, Y., Li, Z., Xing, J., Li, J., 2018. Emission-driven changes in anthropogenic aerosol concentrations in China during 1970–2010 and its implications for $PM_{2.5}$ control policy. Atmos. Res. 212, 106–119.

Chiashi, A., Lee, S., Pollitt, H., Chewpreecha, U., Vercoulen, P., He, Y., Xu, B., 2019. Transboundary PM air pollution and its impact on health in East Asia. In: Lee, S., Pollitt, H., Fujikawa, K. (Eds.), Energy, Environmental and Economic Sustainability in East Asia: Policies and Institutional Reforms. Routledge, London, United Kingdom.

China State Council, 2013. Action plan on prevention and control of air pollution. In: China State Council. China, Beijing.

Dennis, R.L., Bhave, P.V., Pinder, R.W., 2008. Observable indicators of the sensitivity of $PM_{2.5}$ nitrate to emission reductions—Part II: Sensitivity to errors in total ammonia and total nitrate of the CMAQ-predicted non-linear effect of SO_2 emission reductions. Atmos. Environ. 42, 1287–1300.

Dinar, E., Anttila, T., Rudich, Y., 2008. CCN activity and hygroscopic growth of organic aerosols following reactive uptake of ammonia. Environ. Sci. Technol. 42 (3), 793–799.

Draxler, R.R., 1999. HYSPLIT4 user's guide. In: NOAA Tech. Memo. ERL ARL-230. NOAA Air Resources Laboratory, Silver Spring, MD.

Draxler R, R, Rolph, G, 2012. Evaluation of the transfer coefficient matrix (TCM) approach to model the atmospheric radionuclide air concentraions from Fukushima. J. Geophys. Res. 117 (D5). https://doi.org/10.1029/2011JD017205.

Fast, J.D., Gustafson Jr., W.I., Easter, R.C., Zaveri, R.A., Barnard, J.C., Chapman, E.G., Grell, G.A., Peckham, S.E., 2006. Evolution of ozone, particulates, and aerosol direct radiative forcing in the vicinity of Houston using a fully coupled meteorology-chemistry-aerosol model. J. Geophys. Res. 111, D21305.

Finlayson-Pitts, B.J., Hemminger, J.C., 2000. Physical chemistry of airborne sea salt particles and their components. J. Phys. Chem. A 104, 11463–11477.

Fisher, J.A., Jacob, D.J., Wang, Q., Bahreini, R., Carouge, C.C., Cubison, M.J., Dibb, J.E., Diehl, T., Jimenez, J.L., Leibensperger, E.M., Lu, Z., Meinders, M.B.J., Pye, H.O.T., Quinn, P.K., Sharma, S., Streets, D.G., van Donkelaar, A., Yantosca, R.M., 2011. Sources, distribution, and acidity of sulfate-ammonium aerosol in the Arctic in winter-spring. Atmos. Environ. 45, 7301–7318.

Fuzzi, S., Baltensperger, U., Carslaw, K., Decesari, S., Denier van der Gon, H., Facchini, M.C., Fowler, D., Koren, I., Langford, B., Lohmann, U., Nemitz, E., Pandis, S., Riipinen, I., Rudich, Y., Schaap, M., Slowik, J.G., Spracklen, D.V., Vignati, E., Wild, M., Williams, M., Gilardoni, S., 2015. Particulate matter, air quality and climate: lessons learned and future needs. Atmos. Chem. Phys. 15, 8217–8299.

Grell, G.A., Peckham, S.E., Schmitz, R., McKeen, S.A., Frost, G., Skamarock, W.C., Eder, B., 2005. Fully coupled "online" chemistry within the WRF model. Atmos. Environ. 39, 6957–6975.

Guenther, A., Karl, T., Harley, P., Wiedinmyer, C., Palmer, P.I., Geron, C., 2006. Estimates of global terrestrial isoprene emissions using MEGAN (Model of Emissions of gases and Aerosols from Nature). Atmos. Chem. Phys. 6, 3181–3210.

Guo, S., Hu, M., Zamora, M.L., Peng, J., Shang, D., Zheng, J., Du, Z., Wu, Z., Shao, M., Zeng, L., Molina, M.J., Zhang, R., 2014. Elucidating severe urban haze formation in China. Proc. Natl. Acad. Sci. U. S. A. 111, 17373–17378.

Han, S.H., Kim, Y.P., 2015. Long-term Trends of the Concentrations of Mass and Chemical Composition in $PM_{2.5}$ over Seoul. J. Korean Soc. Atmos. Environ. 31 (2), 143–156.

Hassan, S.K., El-Abssawy, A.A., Khoder, M.I., 2013. Characteristics of gas–phase nitric acid and ammonium–nitrate– sulfate aerosol, and their gas–phase precursors in a suburban area in Cairo, Egypt. Atmos. Pollut. Res. 4, 117–129.

Huang, R.J., Zhang, Y., Bozzetti, C., Ho, K.F., Cao, J.J., Han, Y., Daellenbach, K.R., Slowik, J.G., Platt, S.M., Canonaco, F., Zotter, P., Wolf, R., Pieber, S.M., Bruns, E.A., Crippa, M., Ciarelli, G., Piazzalunga, A., Schwikowski, M., Abbaszade, G., Schnelle-Kreis, J., Zimmermann, R., An, Z., Szidat, S., Baltensperger, U., El Haddad, I., Prevot, A.S., 2014. High secondary aerosol contribution to particulate pollution during haze events in China. Nature 514, 218–222.

Jin, Y., Andersson, H., Zhang, S., 2016. Air Pollution Control policies in China: a Retrospective and prospects. Int. J. Environ. Res. Public Health 13, 1219.

Jo, H.Y., Kim, C.H., 2013. Identification of Long-Range Transported Haze Phenomena and their Meteorological Features over Northeast Asia. J. Appl. Meteorol. Climatol. 52 (6), 1318–1328.
Kang, C.M., Lee, H.S., Kang, B.W., Lee, S.K., Sunwoo, Y., 2004. Chemical characteristics of acidic gas pollutants and $PM_{2.5}$ species during hazy episodes in Seoul, South Korea. Atmos. Environ. 38, 4749–4760.
Kang, C.M., Kang, B.W., Lee, H.S., 2006. Source identification and trends in concentrations of gaseous and fine particulate principal species in Seoul, South Korea. J. Air Waste Manage. Assoc. 56 (7), 911–921.
Kim, Y.P., 2006. Air pollution in Seoul caused by aerosols. J. Korean Soc. Atmos. Environ. 22 (5), 535–553.
Kim, B.G., Han, J.S., Park, S.U., 2001. Transport of SO_2 and aerosol over the Yellow Sea. Atmos. Environ. 35, 727–737.
Kim, H.S., Huh, J.B., Hopke, P.K., Holsen, T.M., Yi, S.M., 2007. Characteristics of the major chemical constituents of $PM_{2.5}$ and smog event in Seoul, Korea in 2003 and 2004. Atmos. Environ. 41 (32), 6762–6770.
Kim, C.H., Lee, H.J., Kang, J.E., Jo, H.Y., Park, S.Y., Jo, Y.J., Lee, J.J., Yang, G.H., Park, T., Lee, T., 2018. Meteorological overview and signatures of long-range transport processes during the MAPS-Seoul 2015 campaign. Aerosol Air Qual. Res. 18 (9), 2173–2184.
Krotkov, N.A., McLinden, C.A., Li, C., Lamsal, L.N., Celarier, E.A., Marchenko, S.V., Swartz, W.H., Bucsela, E.J., Joiner, J., Duncan, B.N., Boersma, K.F., Veefkind, J.P., Levelt, P.F., Fioletov, V.E., Dickerson, R.R., He, H., Lu, Z., Streets, D.G., 2016. Aura OMI observations of regional SO_2 and NO_2 pollution changes from 2005 to 2015. Atmos. Chem. Phys. 16, 4605–4629.
Lee, T.H., Choi, J.S., Lee, G.W., Ahn, J.Y., Park, J.S., Atwood, S.A., Schurman, M., Choi, Y.J., Chung, Y.M., Collett Jr., J.L., 2015. Characterization of aerosol composition, concentrations, and sources at Baengnyeong Island, Korea using an aerosol mass spectrometer. Atmos. Environ. 120, 297–306.
Lee, H.J., Jo, H.Y., Park, S.Y., Jo, Y.J., Jeon, W., Ahn, J.Y., Kim, C.H., 2019. A case study of the transport/transformation of air pollutants over the Yellow Sea during the MAPS 2015 campaign. J. Geophys. Res.-Atmos. 124, 6532–6553.
Li, H., Zhang, Q., Zheng, B., Chen, C., Wu, N., Guo, H., Zhang, Y., Zheng, Y., Li, X., He, K., 2018. Nitrate-driven urban haze pollution during summertime over the North China Plain. Atmos. Chem. Phys. 18, 5293–5306.
Lin, M., Oki, T., Bengtsson, M., Kanae, S., Holloway, T., Streets, D.G., 2008. Long-range transport of acidifying substances in East Asia—Part II Source–receptor relationships. Atmos. Environ. 42, 5956–5967.
Liu, F., Zhang, Q., van der Ronald, J., Zheng, B., Tong, D., Yan, L., Zheng, Y., He, K., 2016. Recent reduction in NOx emissions over China: synthesis of satellite observations and emission inventories. Environ. Res. Lett. 11, 114002.
Marcazzan, G.M., Vaccaro, S., Valli, G., Vecchi, R., 2001. Characterisation of PM_{10} and $PM_{2.5}$ particulate matter in the ambient air of Milan (Italy). Atmos. Environ. 35, 4639–4650.
Matsumoto, K., Tanaka, H., 1996. Formation and dissociation of atmospheric particulate nitrate and chloride: an approach based on phase equilibrium. Atmos. Environ. 30, 639–648.
MEE (Ministry of Ecology and Environment of the People"s Republic of China), 2019. China Air Quality Improvement Report (2013–2018).
Mensah, A.A., Buchholz, A., Mentel, T.F., Tillmann, R., Kiendler-Scharr, A., 2011. Aerosol mass spectrometric measurements of stable crystal hydrates of oxalates and inferred relative ionization efficiency of water. J. Aerosol Sci. 42, 11–19.
NCEP (National Centers for Environmental Prediction), 2000. NCEP FNL Operational Model Global Tropospheric Analyses, Continuing from July 1999, Research Data Archive at the National Center for Atmospheric Research. Computational and Information Systems Laboratory.
NIER (National Institute of Environmental Research), 2015. Case Study of High PM Episodes Observed in Intensive Monitoring Station.
NIER (National Institute of Environmental Research), 2017. 2017 NIER Annual Report: Environmental Research, Protecting the People and World.
Ohta, S., Okita, T., 1990. A chemical characterization of atmospheric aerosol in Sapporo. Atmos. Environ. 24, 815–822.
Park, S.U., Lee, E.H., 2003. Long-range transport contribution to dry deposition of acid pollutants in South Korea. Atmos. Environ. 37, 3967–3980.
Park, S.S., Jung, S.A., Gong, B.J., Cho, S.Y., Lee, S.J., 2013. Characteristics of $PM_{2.5}$ haze episodes revealed by highly time-resolved measurements at an air pollution monitoring supersite in Korea. Aerosol Air Qual. Res. 13, 957–976.
Pinder, R.W., Dennis, R.L., Bhave, P.V., 2008. Observable indicators of the sensitivity of $PM_{2.5}$ nitrate to emission reductions—part I: Derivation of the adjusted gas ratio and applicability at regulatory-relevant time scales. Atmos. Environ. 42, 1275–1286.
Rolph, G., Stein, A., Stunder, B., 2017. Real-time Environmental applications and Display sYstem: READY. Environ. Model. Softw. 95, 210–228.
Shapiro, M., 2016. Transboundary Air Pollution in Northeast Asia: The Political Economy of Yellow Dust, Particulate Matter, and $PM_{2.5}$. KEI Academic Paper Series.
Shon, Z.H., Kim, K.H., Song, S.K., Jung, K., Kim, N.J., Lee, J.B., 2012. Relationship between water-soluble ions in $PM_{2.5}$ and their precursor gases in Seoul megacity. Atmos. Environ. 59, 540–550.
Skamarock, W.C., Klemp, J.B., 2008. A time-split nonhydrostatic atmospheric model for weather research and forecasting applications. J. Comput. Phys. 227, 3465–3485.
Squizzato, S., Masiol, M., Brunelli, A., Pistollato, S., Tarabotti, E., Rampazzo, G., Pavoni, B., 2013. Factors determining the formation of secondary inorganic aerosol: a case study in the Po Valley (Italy). Atmos. Chem. Phys. 13, 1927–1939.
Stein, A.F., Draxler, R.R., Rolph, G.D., Stunder, B.J.B., Cohen, M.D., Ngan, F., 2015. NOAA's HYSPLIT atmospheric transport and dispersion modeling system. Bull. Amer. Meteor. Soc. 96, 2059–2077.
Stockwell, W.R., Kuhns, H., Etyemezian, V., Green, M.C., Chow, J.C., Watson, J.G., 2003. The Treasure Valley secondary aerosol study II: modeling of the formation of inorganic secondary aerosols and precursors for southwestern Idaho. Atmos. Environ. 37, 525–534.
Streets, D.G., Bond, T.C., Carmichael, G.R., Fernandes, S.D., Fu, Q., He, D., Klimont, Z., Nelson, S.M., Tsai, N.Y., Wang, M.Q., Woo, J.-H., Yarber, K.F., 2013. An inventory of gaseous and primary aerosol emissions in Asia in the year 2000. J. Geophys. Res.-Atmos. 108.
Tao, J., Zhang, L., Cao, J., Zhang, R., 2017. A review of current knowledge concerning $PM_{2.5}$ chemical composition, aerosol optical properties and their relationships across China. Atmos. Chem. Phys. 17, 9485–9518.
Tian, M., Wang, H.B., Chen, Y., Zhang, L.M., Shi, G.M., Liu, Y., Yu, J.Y., Zhai, C.Z., Wang, J., Yang, F.M., 2017. Highly time-resolved characterization of water-soluble inorganic ions in $PM_{2.5}$ in a humid and acidic mega city in Sichuan Basin. China. Sci. Total Environ. 580, 224–234.
Tian, M., Liu, Y., Yang, F., Zhang, L., Peng, C., Chen, Y., Shi, G., Wang, H., Luo, B., Jiang, C., Li, B., Takeda, N., Koizumi, K., 2019. Increasing importance of nitrate formation for heavy aerosol pollution in two megacities in Sichuan Basin, Southwest China. Environ. Pollut. 250, 898–905.
Wang, Z., Xie, F., Sakurai, T., Ueda, H., Han, Z., Carmichael, G.R., Streets, D., Engardt, M., Holloway, T., Hayami, H., Kajino, M., Thongboonchoo, N., Bennet, C., Park, S.U., Fung, C., Chang, A., Sartelet, K., Amann, M., 2008. MICS-Asia II: model inter-comparison and evaluation of acid deposition. Atmos. Environ. 42 (15), 3528–3542.
Wang, G., Zhang, R., Gomez, M.E., Yang, L., Zamora, M.L., Hu, M., Lin, Y., Peng, J., Guo, S., Meng, J., Li, J., Cheng, C., Hu, T., Ren, Y., Wang, Y., Gao, J., Cao, J., An, Z., Zhou, W., Li, G., Wang, J., Tian, P., Marrero-Ortiz, W., Secrest, J., Du, Z., Zheng, J., Shang, D., Zeng, L., Shao, M., Wang, W., Huang, Y., Wang, Y., Zhu, Y., Li, Y., Hu, J., Pan, B., Cai, L., Cheng, Y., Ji, Y., Zhang, F., Rosenfeld, D., Liss, P.S., Duce, R.A., Kolb, C.E., Molina, M.J., 2016a. Persistent sulfate formation from London fog to Chinese haze. Proc. Natl. Acad. Sci. U. S. A. 113, 13630–13635.
Wang, J., Xu, J., He, Y., Chen, Y., Meng, F., 2016b. Long range transport of nitrate in the low atmosphere over Northeast Asia. Atmos. Environ. 144, 315–324.
Wang, J.D., Zhao, B., Wang, S.X., Yang, F.M., Xing, J., Morawska, L., Ding, A.J., Kulmala, M., Kerminen, V.M., Kujansuu, J., Wang, Z.F., Ding, D.A., Zhang, X.Y., Wang, H.B., Tian, M., Petaja, T., Jiang, J.K., Hao, J.M., 2017. Particulate matter pollution over China and the effects of control policies. Sci. Total Environ. 584-585, 426–447.
Woo, J.H., Quan, S., Choi, K.C., Kim, H., Jin, H., Song, C.K., Han, J.S., Lee, S., 2014. Development of the Comprehensive Regional Emissions Inventory for Atmospheric Transport Experiment (CREATE) inventory in support of integrated modeling of climate and air quality for East Asia. In: In: 16th GEIA Conference. NCAR, Boulder, CO, USA.
Yang, F., Tan, J., Zhao, Q., Du, Z., He, K., Ma, Y., Duan, F., Chen, G., Zhao, Q., 2011. Characteristics of $PM_{2.5}$ speciation in representative megacities and across China. Atmos. Chem. Phys. 11, 5207–5219.
Yang, T., Sun, Y., Zhang, W., Wang, Z., Liu, X., Fu, P., Wang, X., 2017. Evolutionary processes and sources of high-nitrate haze episodes over Beijing. Spring. J. Environ. Sci. 54, 142–151.
Zhang, Q., Jimenez, J.L., Worsnop, D.R., Canagaratna, M., 2007. A case study of urban particle acidity and its influence on secondary organic aerosol. Environ. Sci. Technol. 41, 3213–3219.
Zhang, Q., Geng, G.N., Wang, S.W., Richter, A., He, K.B., 2012. Satellite remote sensing of changes in NOx emissions over China during 1996–2010. Chin. Sci. Bull. 57, 2857–2864.
Zhang, J., Reid, J.S., Alfaro-Contreras, R., Xian, P., 2017. Has China been exporting less particulate air pollution over the past decade? Geophys. Res. Lett. 44, 2941–2948.
Zhao, B., Jiang, J.H., Gu, Y., Diner, D., Worden, J., Liou, K.N., Su, H., Xing, J., Garay, M., Huang, L., 2017. Decadal-scale trends in regional aerosol particle properties and their linkage to emission changes. Environ. Res. Lett. 12, 054021.
Zheng, B., Chevallier, F., Ciais, P., Yin, Y., Deeter, M.N., Worden, H.M., Wang, Y., Zhang, Q., He, K., 2018a. Rapid decline in carbon monoxide emissions and export from East Asia between years 2005 and 2016. Environ. Res. Lett. 13, 044007.
Zheng, B., Tong, D., Li, M., Liu, F., Hong, C., Geng, G., Li, H., Li, X., Peng, L., Qi, J., Yan, L., Zhang, Y., Zhao, H., Zheng, Y., He, K., Zhang, Q., 2018b. Trends in China's anthropogenic emissions since 2010 as the consequence of clean air actions. Atmos. Chem. Phys. 18, 14095–14111.